

“PAIR PRODUCTION OF SCALAR TOP QUARKS IN e^+e^- COLLISIONS AT ILC”

A. Bartl^{a,b}, W. Majerotto^c,
K. Mönig^d, A.N. Skachkova^e, N.B. Skachkov^e

August 12, 2021

^a *University of Vienna, Faculty of Physics, 1090 Vienna, Boltzmannngasse 5, Austria.*

^b *AHEP Group, Instituto de Fisica Corpuscular - C.S.I.C., Universidad de Valencia, Edificio Institutos de Investigacion, Apt. 22085, E-46071 Valencia, Spain*

^c *Institute for High Energy Physics (HEPHY Vienna), Nikolsdorfergasse 18, A-1050 Vienna, Austria.*

^d *DESY, Platanenallee 6, D-15738 Zeuthen, Germany.*

^e *JINR, Joliot-Curie 6, 141980 Dubna, Moscow region, Russia.*

Abstract

We study the pair production of scalar top quarks \tilde{t}_1 in e^+e^- collisions with the subsequent decay into b -quarks and charginos, $\tilde{t}_1 \rightarrow b\tilde{\chi}_1^\pm$. We simulate this process using PYTHIA6.4 for beam energies $2E_{beam} = \sqrt{s} = 350, 400, 500, 800, 1000$ GeV. Proposing a set of criteria we obtain a good separation of the signal stop events from top quark pair production which is the main background. The number of stop production events obtained with the proposed cuts for different energies is calculated for an integrated luminosity of $1000 fb^{-1}$. We propose a method to reconstruct the mass of the top squark, provided the mass of the lightest neutralino is known, and estimate the error of the mass determination for the case $\sqrt{s} = 500$ GeV.

1 Introduction.

The scalar top quark, the bosonic partner of the top quark, has attracted much attention as it is expected to be the lightest colored supersymmetric (SUSY) [1] particle. \tilde{t}_L and \tilde{t}_R , the supersymmetric partners of the left-handed and right-handed top quark, mix and the resulting two mass eigenstates \tilde{t}_1 and \tilde{t}_2 , can have a large mass splitting. It is even possible that the lighter eigenstate \tilde{t}_1 could be lighter than the top quark itself [2], [3].

Searches for top squarks were performed at LEP and Tevatron and will continue at LHC and ILC [4], [5].

This Note is the continuation of our previous Note where we have considered stop pair production in photon-photon collisions [6]. In the following we study the reaction

$$e^+ + e^- \rightarrow \tilde{t}_1 + \tilde{t}_1^* \quad (1)$$

Among the possible \tilde{t}_1 -decay channels within the MSSM (see [7] for details), we focus on the decay $\tilde{t}_1 \rightarrow b\tilde{\chi}_1^\pm$ followed by the two-body chargino decay $\tilde{\chi}_1^\pm \rightarrow \tilde{\chi}_1^0 W^\pm$, where one of the W 's decays hadronically, $W \rightarrow q_i \bar{q}_j$, and the other one leptonically, $W \rightarrow \mu \nu_\mu$ ¹ [8]. The final state of this signal process, shown in the left diagram of Fig.1, contains two b - quarks, two quarks (originating from the decay of one W boson), a hard muon plus a neutrino (from the decay of the other W) and two neutralinos:

$$e^+ e^- \rightarrow \tilde{t}_1 \tilde{t}_1^* \rightarrow b \bar{b} \tilde{\chi}_1^+ \tilde{\chi}_1^- \rightarrow b \bar{b} W^+ W^- \tilde{\chi}_1^0 \tilde{\chi}_1^0 \rightarrow b \bar{b} q_i \bar{q}_j \mu \nu_\mu \tilde{\chi}_1^0 \tilde{\chi}_1^0. \quad (2)$$

The main background process is top quark pair production with the subsequent decay $t \rightarrow bW^\pm$ (for W 's we use the same decay channels as in the stop case):

$$e^+ e^- \rightarrow t \bar{t} \rightarrow b \bar{b} W^+ W^- \rightarrow b \bar{b} q_i \bar{q}_j \mu \nu_\mu. \quad (3)$$

The only difference between the final states of stop and top production (shown in the right diagram of Fig.1) is that in stop pair production there are two neutralinos which are undetectable. Thus, both processes have the same signature: two b -jets, two jets from W decay and a muon. In the following we show that the physical variables constructed of jets combinations may allow to reconstruct the scalar top quark mass.

In the present paper we consider only top pair production as background. We analyse

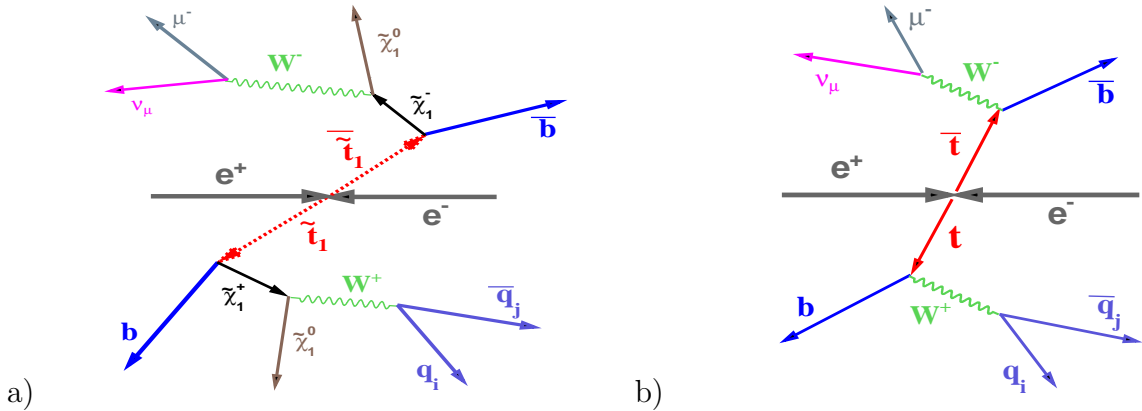


Figure 1: *Left is the stop signal event diagram, Right is the top background diagram.*

the processes (2) and (3) with the help of Monte Carlo samples of the corresponding events generated by the two programs PYTHIA6.4 [12] and CIRCE1 [13]. The program CIRCE1 is used for the parametrization of the beam spectra involved in the processes (2) and (3) to account for the effects of beamstrahlung. The energy of the beams is chosen as $2E_{beam} = \sqrt{s} = 350, 400, 500, 800, 1000$ GeV. Most plots are shown for $\sqrt{s} = 500$ GeV and a stop mass $M_{\tilde{t}_1} = 167.9$ GeV.

¹ The process $e^+ e^- \rightarrow \tilde{t}_1 + \tilde{t}_1^*$ with the subsequent decay $\tilde{t}_1 \rightarrow c\tilde{\chi}_1^0$ was considered in [9]–[11].

In Section 2 we give the set of MSSM parameters used in our study.

In Section 3 we discuss some general characteristics of the signal process $e^+e^- \rightarrow \tilde{t}_1\tilde{t}_1$ and the main background $e^+e^- \rightarrow t\bar{t}$. First we show how the beam energies are affected by beamstrahlung and other beam interaction effects which are simulated with CIRCE1. The subsections include kinematical distributions (obtained without imposing of any cuts) for the produced stop quarks, for the jets originating from W boson decay and for b -jets. We compare them in detail with those of top pair production.

In Section 4 we demonstrate how to discriminate between the signal muons produced in W boson decays and those stemming from hadron decays in the same events.

In Section 5 we show the distributions of the global variables missing energy, total visible energy, the scalar sum of the transverse momenta of all visible particles in the event and the invariant masses of the final-state hadronic jets plus the signal muon. We show that they are good tools for separating the signal from the top background.

In Section 6 we introduce further two global variables, the invariant mass of the final-state hadronic jets and the missing mass and demonstrate that they are very useful for the separation of signal stop events from the background top events. We propose three cuts which provide a good signal-to-background ratio (S/B). The impact of the proposed cuts on the values of the cross sections of stop and top pair productions are shown together with the values of S/B ratios for different values of \sqrt{s} .

Section 7 is devoted to the mass reconstruction of the scalar top quark based on the distribution of the invariant mass of one b -jet and the other two *non* - b -jets (from W decay), provided that the neutralino mass is known.

In Section 8 we show the distributions of the invariant variables described in Section 7 for a stop mass $M_{\tilde{t}_1} = 200$ GeV.

Section 9 contains some conclusions.

2 MSSM parameters and cross section.

The scalar top quark system is described by the mass matrix (in the $\tilde{t}_L - \tilde{t}_R$ basis) [2], [14]

$$\begin{pmatrix} M_{\tilde{t}_{LL}}^2 & M_{\tilde{t}_{LR}}^2 \\ M_{\tilde{t}_{RL}}^2 & M_{\tilde{t}_{RR}}^2 \end{pmatrix} \quad (4)$$

with

$$M_{\tilde{t}_{LL}}^2 = M_Q^2 + \left(\frac{1}{2} - \frac{2}{3}\sin^2\Theta_W\right)\cos 2\beta M_Z^2 + M_t^2, \quad (5)$$

$$M_{\tilde{t}_{RR}}^2 = M_U^2 + \frac{2}{3}\sin^2\Theta_W\cos 2\beta M_Z^2 + M_t^2, \quad (6)$$

$$M_{\tilde{t}_{RL}}^2 = (M_{\tilde{t}_{LR}}^2)^* = M_t(A_t - \mu^*\cot\beta). \quad (7)$$

The mass eigenvalues are given by

$$M_{\tilde{t}_{1,2}}^2 = \frac{1}{2} \left[(M_{\tilde{t}_{LL}}^2 + M_{\tilde{t}_{RR}}^2) \mp \sqrt{(M_{\tilde{t}_{LL}}^2 - M_{\tilde{t}_{RR}}^2)^2 + 4|M_{\tilde{t}_{LR}}^2|^2} \right] \quad (8)$$

with the mixing angle

$$\cos\theta_{\tilde{t}} = \frac{-M_{\tilde{t}_{LR}}^2}{\sqrt{|M_{\tilde{t}_{LR}}^2|^2 + (M_{\tilde{t}_1}^2 - M_{\tilde{t}_{LL}}^2)^2}} \quad (9)$$

$$\sin\theta_{\tilde{t}} = \frac{M_{\tilde{t}_{LL}}^2 - M_{\tilde{t}_1}^2}{\sqrt{|M_{\tilde{t}_{LR}}^2|^2 + (M_{\tilde{t}_1}^2 - M_{\tilde{t}_{LL}}^2)^2}} \quad (10)$$

In the following we will consider a particular choice of the MSSM parameters that are defined, in the notations of PYTHIA6.4, in the following way:

$$M_{\tilde{Q}} = 270 \text{ GeV}; \quad M_{\tilde{U}} = 270 \text{ GeV}; \quad A_t = -500 \text{ GeV} \text{ (stop trilinear coupling);}$$

$$\tan\beta = 5; \quad \mu = -370 \text{ GeV}; \quad M_1 = 80 \text{ GeV}; \quad M_2 = 160 \text{ GeV}.$$

Note that in PYTHIA6.4 $M_{\tilde{Q}}$ corresponds to $M_{\tilde{t}_L}$ (left squark mass for the third generation) and $M_{\tilde{U}}$ corresponds to $M_{\tilde{t}_R}$. These parameters give $M_{\tilde{t}_1} = 167.9 \text{ GeV}$, $M_{\chi_1^+} = 159.2 \text{ GeV}$ and $M_{\chi_1^0} = 80.9 \text{ GeV}$. This parameter point is compatible with all experimental data. We have chosen this value of $M_{\tilde{t}_1}$ rather close to the mass of the top quark $M_{top} = 170.9 \pm 1.8 \text{ GeV}$ [15]. This means that one expects a rather large contribution from the top background, therefore, this choice makes the analysis most difficult. Finding a suitable set of cuts separating stop and top events is crucial.

In general, the cross section for stop pair production at a fixed energy depends on the mass of the stop quark and the mixing angle $\theta_{\tilde{t}}$. Since the couplings of the Z^0 to the left and right components of the stop are different, the cross sections depend significantly on the beam polarizations (see [7], [8], [22]). By choosing appropriate longitudinal beam polarizations it is possible to enhance the cross sections. For example, for an electron beam with 90% left polarization the cross section would be larger than the unpolarized cross section by approximately 40%, for $\cos\theta_{\tilde{t}} = -0.81$ corresponding to the parameters given above. If in addition the positron beam has 60% right polarization, then the cross section is enhanced by approximately a factor of 2 compared to the unpolarized cross section. We note that a rather precise determination of the stop mixing angle $\theta_{\tilde{t}}$ is possible by measuring the left-right asymmetry. The cross section for top pair production has also a characteristic dependence on the beam polarizations [22]. For example, the polarization of both beams leads to an increase of the cross section by about a factor of 1.5.

3 Distributions of kinematical variables in stop and top production.

In the following we present some distributions of different physical variables based on the sample of $5 \cdot 10^4$ stop pair production events generated by PYTHIA6.4 and CIRCE1 weighted with the electron-positron luminosity. Analogous plots are also given for 10^6 generated background top events. In this Section all plots are obtained without any cuts.

The ILC is a linear electron-positron collider with a center-of-mass energy of 200-500 GeV and a high luminosity (peak luminosity of $\sim 2 \cdot 10^{34} \text{ cm}^{-2} \text{ s}^{-1}$), upgraded to 1 TeV in the second phase. According to [4] a total luminosity of 500 fb^{-1} is foreseen within the first four years of operation and 1000 fb^{-1} during the first phase of operation at 500 GeV. A first run at $\sqrt{s} = 500 \text{ GeV}$ will get a first measurement of the particle masses to optimize the threshold scan [5].

Fig.2 a) demonstrates the total energy spectrum of the electron and positron beams $E1_{e^+} + E2_{e^-}$, which is expected at $2E_{beam} = \sqrt{s} = 500 \text{ GeV}$ after taking into account

beamstrahlung and other beam interaction effects (see, for instance [23]). Fig.2 b) shows the correlations of the beam energy fractions $y_i = E_i/E_{beam}$ ($i=e^+, e^-$) of the colliding electron and positron beams.

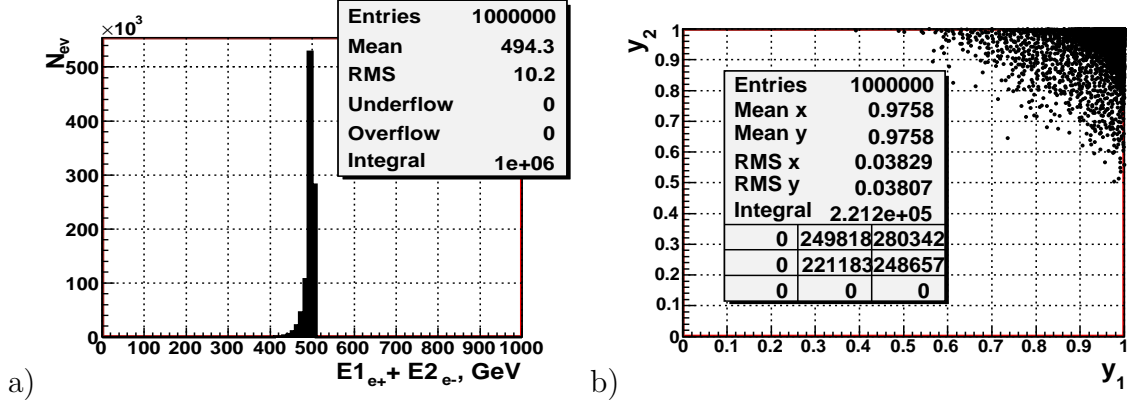


Figure 2: a) total beam energy spectrum, b) beam fractions correlations.

3.1 Distributions in stop events.

In Sections 3, 4 and 5 we will present plots for the kinematical distributions only for the energy $\sqrt{s} = 500$ GeV. Fig.3 shows two kinematical distributions characteristic of the produced stop pair system, i.e., the number of expected events versus the stop transverse momentum $PT_{t_1}^{\sim}$ (plot a)) and its polar angle $\theta_{t_1}^{\sim}$ (see plot b)) (all in the e^+e^- c.m.s.). As can be seen in Fig.3 a) the stop transverse momentum $PT_{t_1}^{\sim}$ spectrum begins at $PT_{t_1}^{\sim} \approx 50$ GeV and has a peak near the kinematical limit.

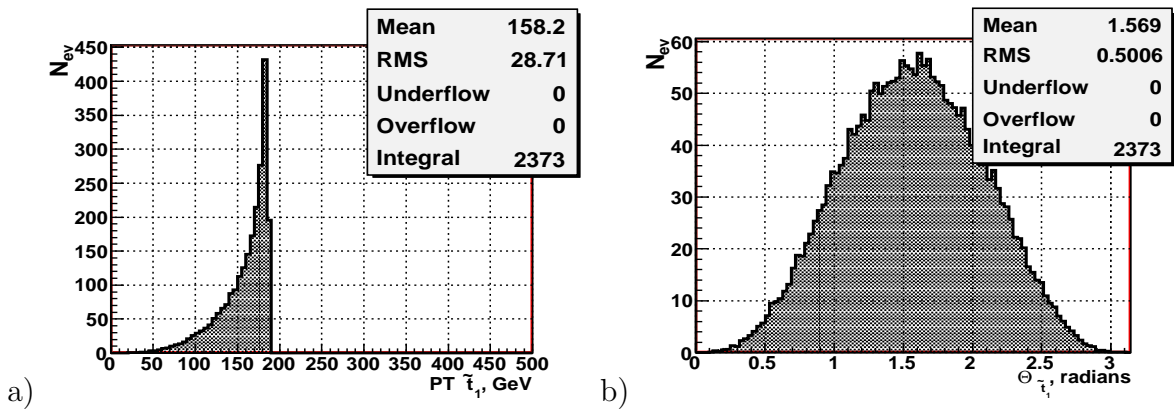


Figure 3: Distributions of the number of events N_{event} ($L_{int} = 1000 fb^{-1}$) versus: a) stop transverse momentum $PT_{t_1}^{\sim}$; b) stop polar angle $\theta_{t_1}^{\sim}$.

In Fig.3 and the following figures the vertical axis shows the number of stop and top events that may be expected for the integrated luminosity $L_{int} = 1000 fb^{-1}$. Taking the integral of the distributions one can get the total number of events expected for this luminosity. These numbers are shown as "Integral" values in the Figures.

To find the jets we use the subroutine PYCLUS of PYTHIA with the distance measure utilized in the "Durham algorithm". The parameters of this jet finder, which is widely used in e^+e^- physics, are chosen such that the number of jets is *exactly* four (see also [18]).

3.2 Distributions of the jets from W decay.

According to the decay chain (2), the final state has to contain two jets due to the decay of one W boson into two quarks $W \rightarrow q_i + \bar{q}_j$ (see Fig.1).

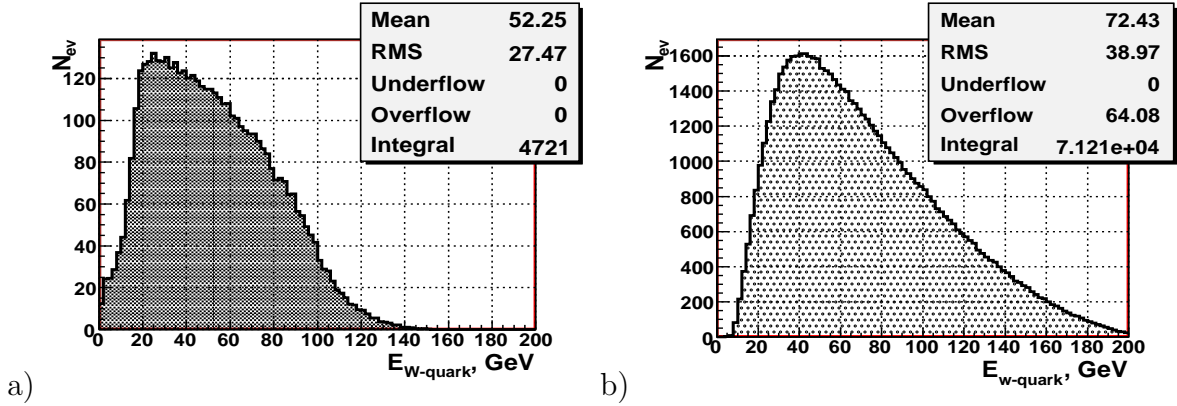


Figure 4: *Energy spectra of the quarks from W boson decay. a) stop pair production; b) top pair production.*

Plot a) (for stop pair production) and plot b) (for top pair production) of Fig.4 show the distributions of the energy $E_{W-quark}$ of the quarks produced in the W boson decay (which we call "W-quarks"). The first spectrum begins at zero and goes up to 140 GeV, with a mean value of 52 GeV, while the second spectrum begins around 8 GeV and goes up to approximately 200 GeV, with a mean value of 72 GeV.

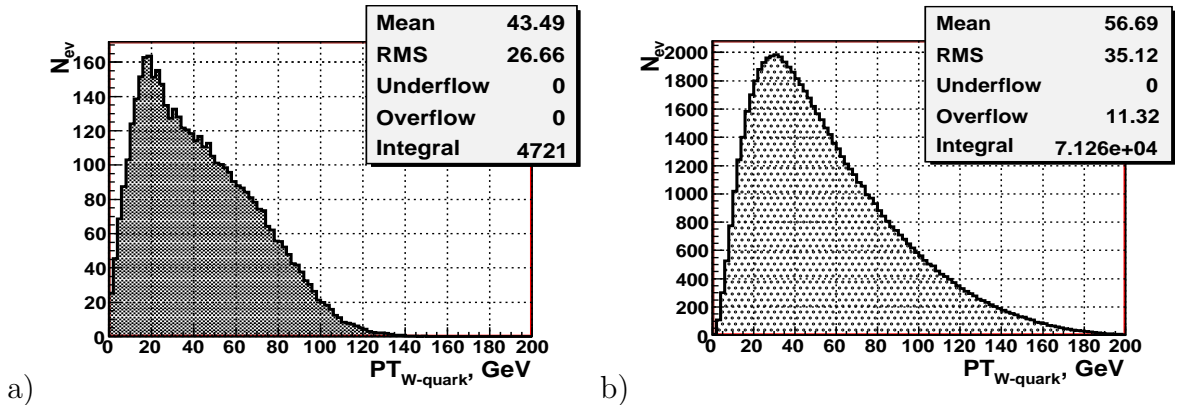


Figure 5: *PT spectra of the quarks produced in the W boson decay. a) stop pair production; b) top pair production.*

Figure 5 shows the transverse momentum $PT_{W-quark}$ spectra of the quarks produced in the W boson decay for stop (plot a)) and top (plot b)) production. The shapes of the

$PT_{W-quark}$ spectra of these "W-quarks" are rather similar to the $E_{W-quark}$ spectra. In the case of top production the "W-quarks" are slightly more energetic and have a larger transverse momentum than those from stop pair production.

As the next step we take into account the hadronization of the "W-quark" into a jet which we call " jet_W ". Figs.6 and 7 show the energy E_{jet_W} and transverse momentum PT_{jet_W} distributions of the corresponding "W-jets". Plots a) and b) are for stop and top production, respectively. According to our choice of PYCLUS jet finder parameters there are two " jet_W " in the event.

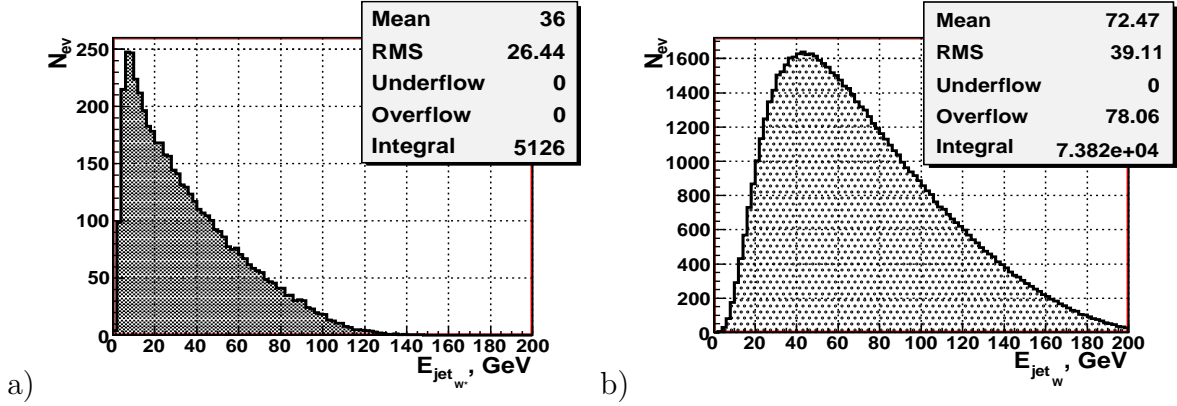


Figure 6: E_{jet_W} energy spectra. a) stop pair production; b) top pair production.

Comparing plot a) of Fig.6 for the energy distribution of "W-jets" in stop production with the plot a) of Fig.4 one observes that the corresponding mean value of the "W-jets" energy $E_{jet_{W^*}}$ (we use the notation W^* in the stop case, for some details see below) in Fig.6 is about 16 GeV lower than the mean energy $E_{W-quark}$ of "W-quarks". It is also seen (plot a) of Fig.4) that the peak position of "W-quark" energy distribution ($E_{W-quark}^{peak} \approx 25$ GeV) is shifted to the left by about 17 GeV ($E_{jet_{W^*}}^{peak} \approx 8$ GeV) when passing to the jet level (see plot a) of Fig.6). The end point of the $E_{jet_{W^*}}$ distribution in stop case is somewhat lower than that one for the corresponding quarks.

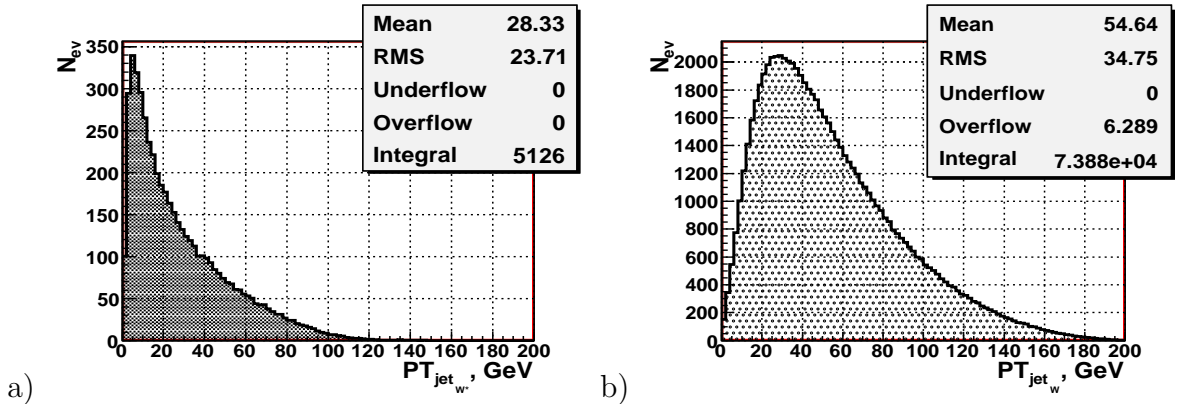


Figure 7: " jet_W " PT - spectra. a) stop pair production; b) top pair production.

Analogously, the mean value and the peak position of the distribution of the transverse momentum of the "W*-quarks", $PT_{W^*-quark}$, shown in Fig.5 a), decrease by about 13-15

GeV when passing to the jet level (see Fig.7 a)), while the end point of the PT_{jetW^*} distribution is a bit lower than the end point of $PT_{W^*-quark}$ distribution.

Due to the different kinematics in top production mentioned above, the energy E_{jetW} , its peak position and the mean value of the "jet $_W$ " energy distribution in the top case are practically equivalent to the $E_{W-quark}$ spectrum, peak position and the mean value of the corresponding "W-quark" energy distribution (see Fig.4 b) and Fig.6 b)). Analogously, by comparing plots b) of Figs. 5 and 7 for $PT_{W-quark}$ and PT_{jetW} , one can see that the transverse momentum distribution in top production is stable under hadronization.

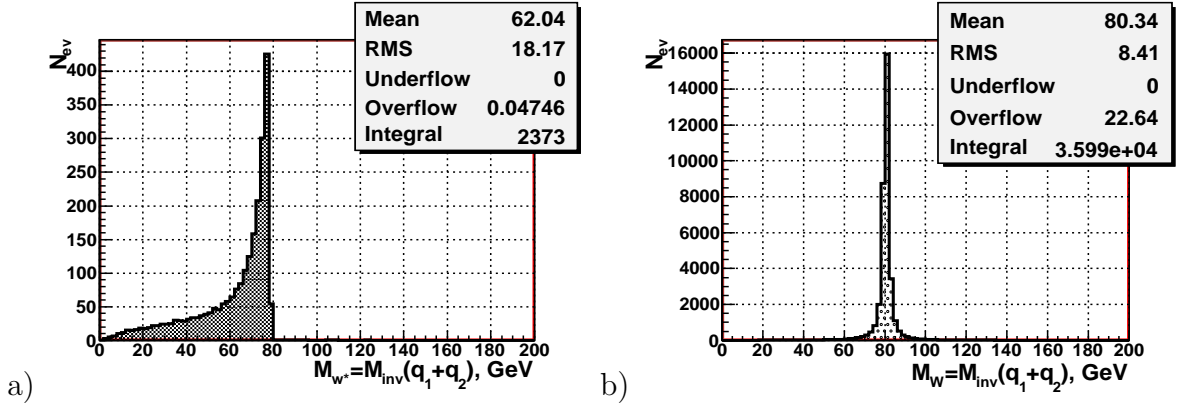


Figure 8: The invariant mass of two quarks $M_W = M_{inv}(quark1 + quark2)$, reconstructed from the vectorial sum of 4-momenta of two quarks that are produced in $W \rightarrow q_i + \bar{q}_j$ decay. a) stop pair production; b) top pair production.

Figure 8 shows the spectrum of the invariant mass $M_{inv}(quark_i + quark_j) \equiv M_W$ reconstructed from the vectorial sum of 4-momenta of the two quarks produced in W decay $W \rightarrow q_i \bar{q}_j$. Plot a) is for stop pair production, plot b) is for top pair production. In plot a) of Fig.8 one clearly sees the virtual nature of the W boson in the stop pair production case which we denote by a (*) in W^* . Hence, in the stop case the invariant mass of two quarks produced in the decay of the virtual W^* is smaller than the mass of a real W boson. In top production (see plot b) of Fig.8) there is a peak in the invariant mass distribution at the mass value of the real W boson.

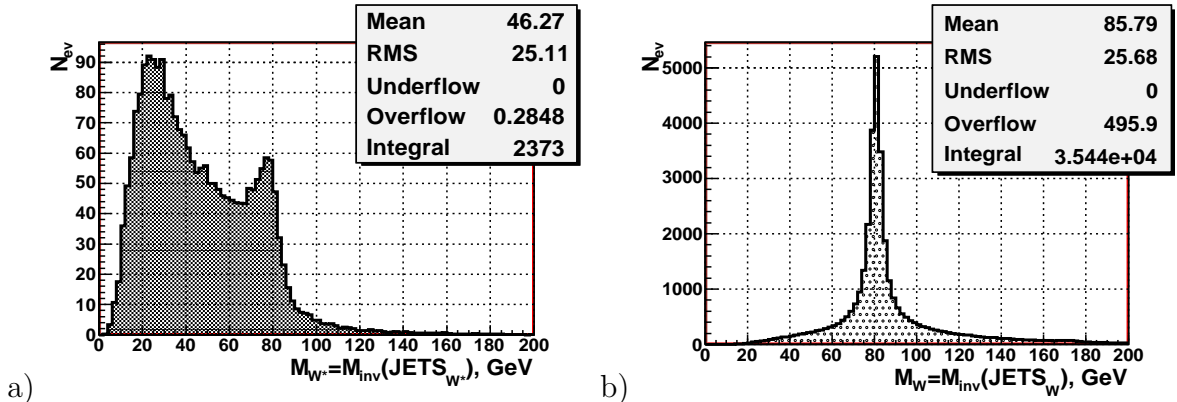


Figure 9: Number of generated events versus the reconstructed invariant mass of "all-non-b-jets". a) stop pair production; b) top pair production.

Figure 9 shows the corresponding plots at the jet level. The invariant mass in Fig.9 is built of two "jet_W" - jets produced in the W boson decay (or, shortly, "JETS_W"). One can see from plot **a**) that in the stop case the spectrum of the invariant masses $M_{W^*} \equiv M_{inv}(JETS_{W^*})$ is strongly shifted to the left. It has the main peak in the interval from 20 to 30 GeV and two tails. The left tail is rather short while the right one is very long and it spreads up to $M_{W^*} \approx 180$ GeV. There is another not so high peak of, approximately, 65% of the height of the main peak, which is seen near the position of the peak shown in the quark level plot **a**) of Fig.8 near the point $M_{W^*} = 80$ GeV. As seen from plot **b**), in the top case the position of the W-peak at the jet level remains (with a high precision) at the same value of M_W as at the quark level in plot **b**) of Fig.8. There appear a shift in the mean value (about 6 GeV) and some tails on both sides.

3.3 *b*-quark and *b*-jet distributions in stop and top production.

In the case of stop decay into a *b*-quark and a chargino, $\tilde{t}_1 \rightarrow b\tilde{\chi}_1^\pm$, the jets produced in *b*-quark hadronization are observable objects. Their features are interesting from the viewpoint of experimentally distinguishing the stop signal events from the top background.

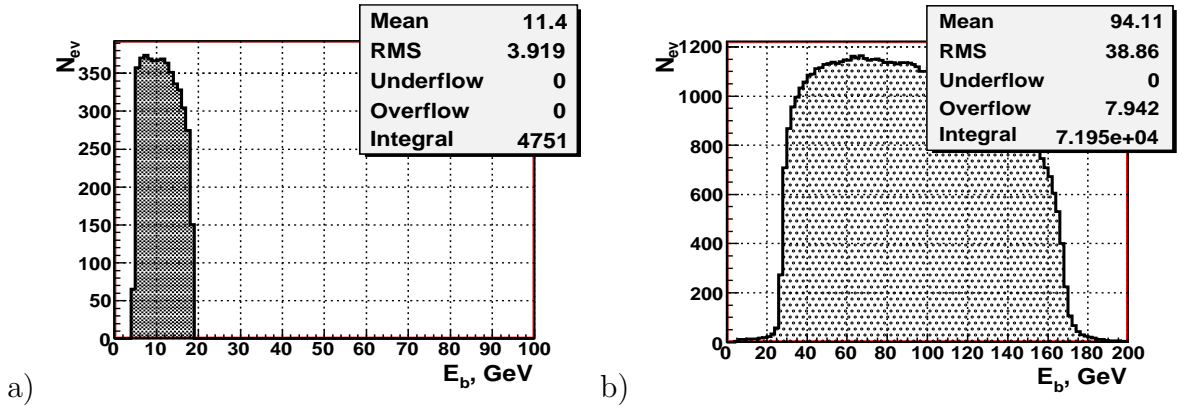


Figure 10: *b*- and \bar{b} -quark energy spectra. **a**) stop pair production; **b**) top pair production.

In Fig.10 we show in plot **a**) for stop pair production and plot **b**) for top pair production the distributions of the energies E_b of the *b*- and \bar{b} -quarks (which we do not distinguish in the following) produced in stop and top decay chains (2) and (3), respectively. Both spectra begin at $E_b \approx 4$ GeV, corresponding to the *b*-quark mass, but look very different. The *b*-quark energy spectrum in stop production strongly increases up at $E_b \approx 4$ GeV and strongly decreases at $E_b \approx 17-19$ GeV. The corresponding spectrum in top production is much harder and its main part is concentrated within the interval $25 < E_b < 170$ GeV. The mean values of the *b*-quark energies are about 11 GeV and 94 GeV in stop and top production, respectively. This means that in the stop case (see plot **a**)) the *b*-quark takes a smaller part of the stop energy $E_{\tilde{t}_1} \approx 250$ GeV than the *b*-quark gets in the background top case (see plot **b**)).

Figure 11 shows the transverse momentum PT_b spectra of *b*-quarks for stop (plot **a**)) and top (plot **b**)) production. Comparing plot **a**) of Fig.11 with plot **a**) in Fig.3, one can conclude that in stop pair production the *b*-quarks have only a small fraction of the transverse momentum of the parent stops. The shape of the PT_b spectrum of *b*-quarks in

the stop case (see plot **a**) in Fig.11) is similar to the shape of the E_b spectrum (see plot **a**) in Fig.10). This means that in the stop decay the transverse component of the b -quark momentum is larger than the longitudinal component.

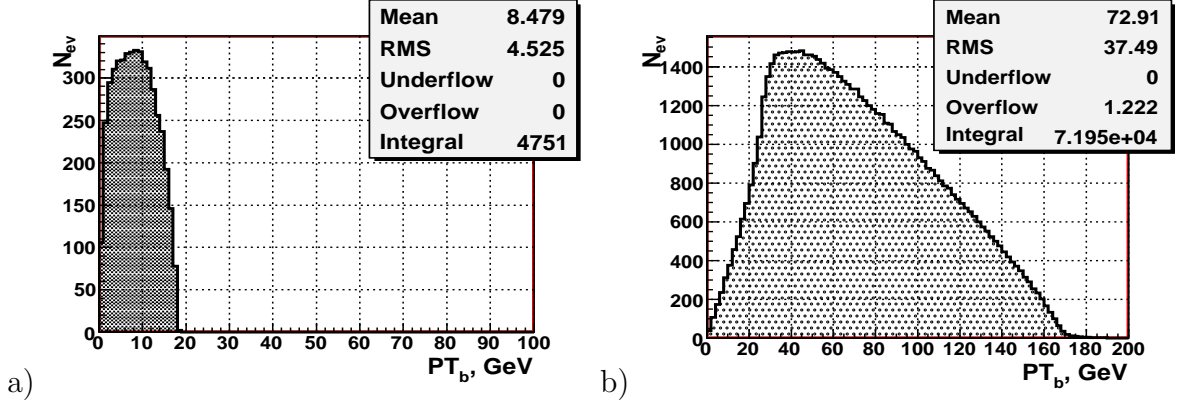


Figure 11: b - and \bar{b} -quark PT spectra. **a)** stop pair production; **b)** top pair production.

The kinematical distributions of the b -quarks in top decay are quite different. As seen from plots **b)** of Fig.10 and Fig.11, the b -quarks produced in the top decays are very energetic. Most of the top events have $E_b \geq 25$ GeV and $PT_b \geq 20$ GeV. The difference to stop decay is easily understandable. The stop decays into a heavy chargino, whereas the top decays into a real W boson whose mass is only half of the mass of the chargino $M_{\chi_1^\pm}$. Therefore, the b -quarks in top decays have a larger phase space than the b -quarks in stop decays.

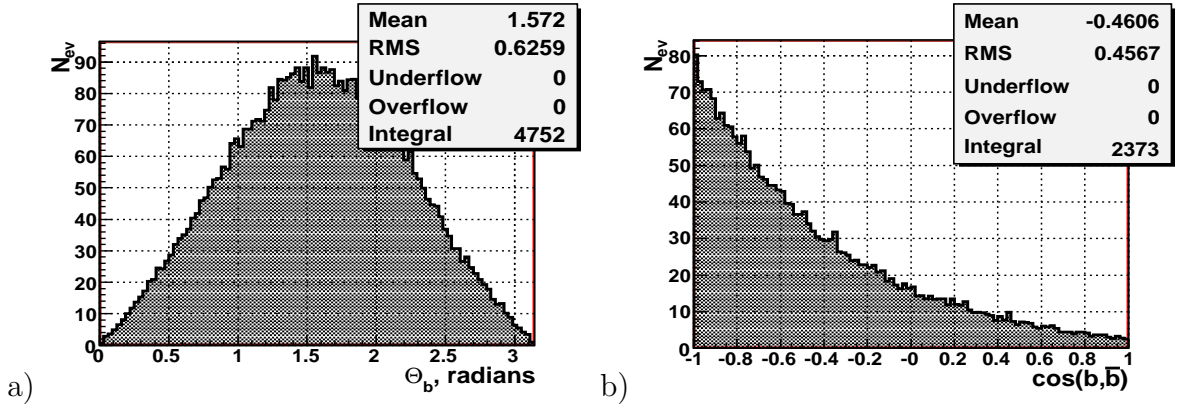


Figure 12: **a)** b - and \bar{b} -quark polar angle Θ_b distribution in stop production; **b)** $\cos(b, \bar{b})$ distribution in stop production.

The distribution of the polar angle Θ_b of the b -quarks in stop production is presented in plot **a)** of Fig.12. Plot **b)** of Fig.12 contains the $\cos(b, \bar{b})$ distribution, where $\cos(b, \bar{b})$ is the cosine of the opening angle between the 3-momenta of the b - and \bar{b} -quarks produced in the same stop event. It demonstrates that most of the b - and \bar{b} -quarks move in approximately opposite directions, but some are in the same hemisphere. Thus in the experiment we may expect a similar angular distributions of the corresponding b - and \bar{b} - jets.

As the next step, we take into account b -quark hadronization into a b -jet. Technically, b -jets are defined as jets that contain at least one B-hadron. Their decay may be identified by the presence of a secondary vertex [19].

Figs.13 and 14 show the energy E_{b-jet} and transverse momentum PT_{b-jet} distributions of the corresponding b -jets. Plots a) and b) are for stop and top production, respectively.

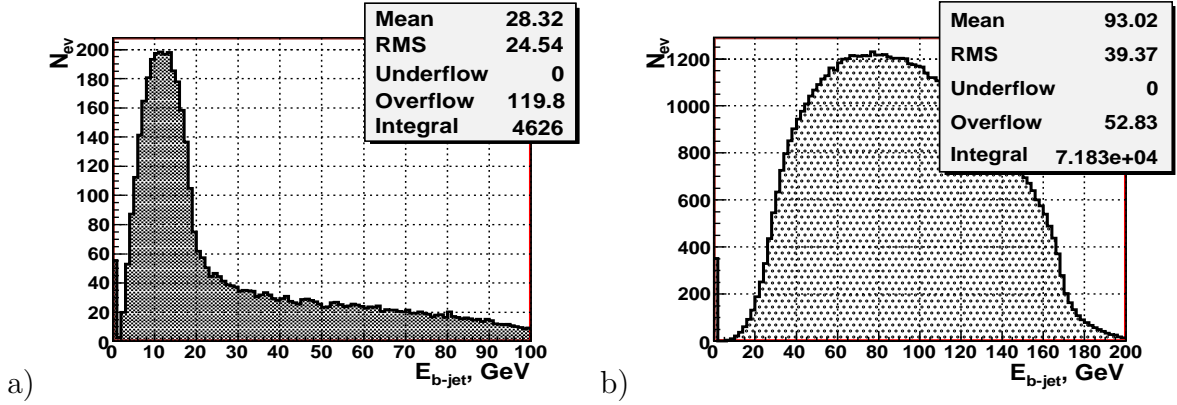


Figure 13: b -jet energy spectra. a) stop pair production; b) top pair production.

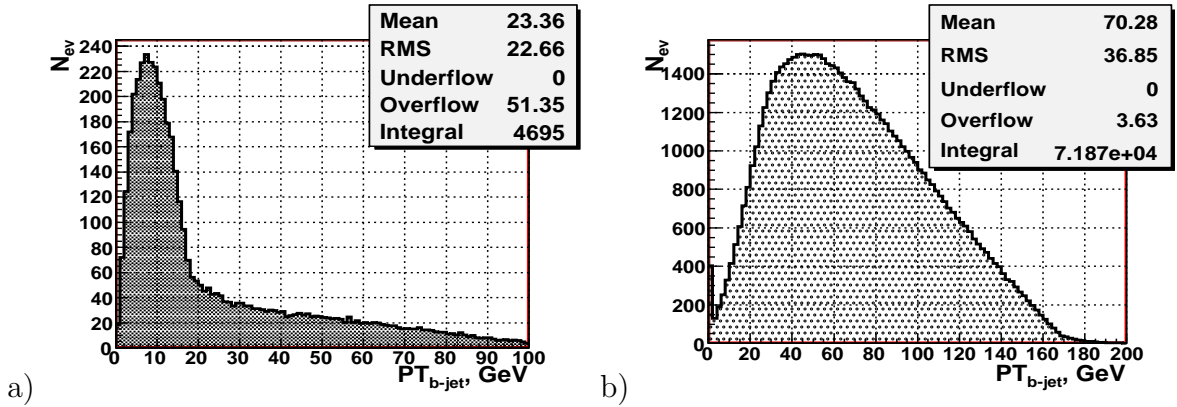


Figure 14: b -jet PT - spectra. a) stop pair production; b) top pair production.

Comparing plots a) of Figs.13 and 14 for the b - and \bar{b} -jet energy E_{b-jet} and jet transverse momentum PT_{b-jet} distributions in stop production with the Figs.10 a) and 11 a), one observes that the corresponding mean values of jet energy and transverse momentum are about 15-17 GeV higher than those for the quarks. The reason for this is that in the stop case the end points of the energy distributions for the b -jets and \bar{b} -jets are higher than those for the corresponding quarks due to appearance of long tails at higher E_{b-jet} .

It is worth emphasizing that at the same time the position of the peak in b -jet energy distribution E_{b-jet} (see plot a) of Fig.13) in the stop case is only slightly shifted to higher values (by about 3-4 GeV) compared to the E_b peak in plot a) of Fig 10. Also note that there are practically no changes of the peak positions of the quark level PT_b and the jet level PT_{b-jet} distributions shown in plots a) of Figs.11 and 14, respectively. Thus we can say that the peak positions of energy and transverse momentum distributions turn out to be rather stable when passing from b -quark to b -jet level.

Now let us turn to the analogous energy and transverse momentum distributions obtained for the case of top background. As seen from comparison of the energy plots **b)** of Figs.10 and 13, as well as the transverse momentum plots **b)** of Figs.11 and 14, the mean values of the b -jet and \bar{b} -jet energy and transverse momentum distributions are about 1-3 GeV smaller than the mean values of the corresponding b -quark and \bar{b} -quark distributions.

Let us summarize the results which were obtained in subsections 3.2 and 3.3 by the use of PYCLUS jet finder. First, it was found that in the case of top background production the characteristic parameters of energy and transverse momentum distributions of jets stemming from W decay and of b -jets, produced in b -quark hadronization, practically do not differ from the parameters of their parent quarks distributions.

This picture changes quite noticeably when we consider the case of stop production with its further decay through the channel $\tilde{t}_1 \rightarrow b\tilde{\chi}_1^\pm$. In this case the b -quarks are much less energetic than the b -quarks produced in top decay $t \rightarrow bW^\pm$. It was observed that the use of the same PYCLUS jet finder in the stop case leads to a noticeable redistribution of jet energies and, correspondingly, of their transverse momentum. Namely, the mean values of jet energy E_{jetW^*} and jet transverse momentum PT_{jetW^*} are about 15-17 GeV smaller than the energy $E_{W-quark}$ and transverse momentum $PT_{W-quark}$ of parent "W-quarks" (stemming from W boson decay), while the mean values of b -jet energy E_{b-jet} and jet transverse momentum PT_{b-jet} are by about 15-17 GeV higher than the energy E_b and PT_b of parent b -quarks.

In the following we shall return to this subject and consider the set of physical variables which shall take into account this effect of energy redistribution in a case of stop production.

4 Distributions of the signal muons.

To select the signal stop pair production events shown in the left diagram of Fig.1 one has to identify the muon from the W decay. The corresponding energy E_{sig-mu} and transverse momentum PT_{sig-mu} distributions of the signal muons are shown in Fig.15.

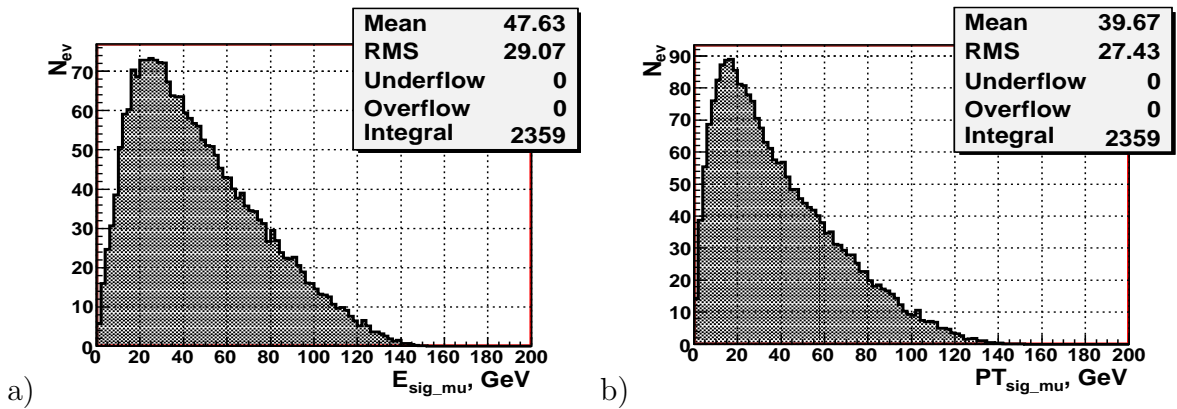


Figure 15: **a)** Energy distributions of signal muons. **b)** PT distributions of signal muons.

There are, however, also muons in the event coming from leptonic and semileptonic

decays of hadrons. Fig.16 **a)** and **b)** show, respectively, the energy E_{dec-mu} and the transverse momentum PT_{dec-mu} spectra of these background muons stemming from hadron decays within the detector volume (for which we took the size from [4], [5]). It can be seen that the decay muons have a rather small energy E_{dec-mu} and transverse momentum PT_{dec-mu} . Their mean values are about 0.79 and 0.63 GeV, respectively. The analogous spectra for the signal muons in Fig.15 show that the signal muons have a much higher energy E_{sig-mu} and transverse momentum PT_{sig-mu} . The mean value of the signal muons energy $E_{sig-mu}^{mean} = 47.6$ GeV is about 60 times higher than the mean value of the energy of the decay muons. An analogous difference can be seen between the mean values of transverse momenta PT of signal and decay muons. One can cut off most low-energy decay muons rejecting those with $E_{mu} \leq 4$ GeV. Such a cut leads to a loss of about 15-20 signal events as seen from the plot **a)** of Fig.15 (the bin width in this plot is 2 GeV).

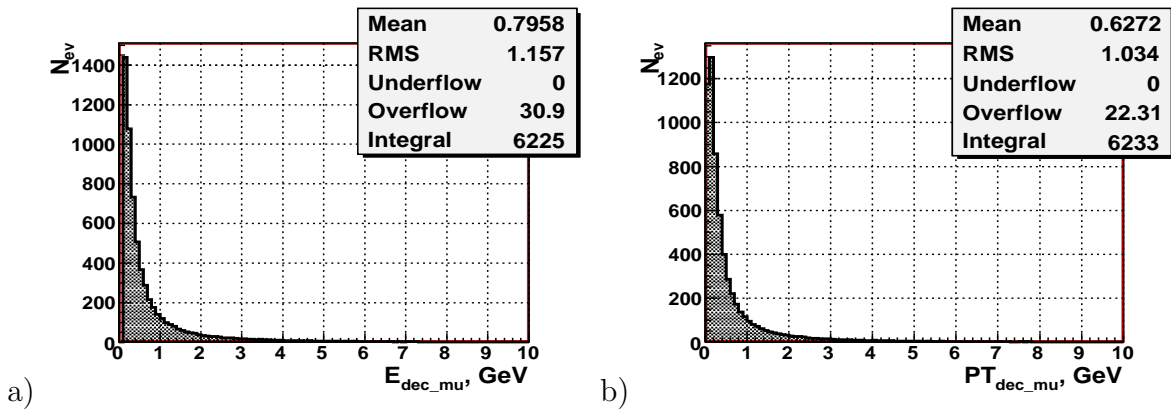


Figure 16: *Distributions of background muons. a) Energy distribution; b) PT distribution.*

We have also studied another way to select the signal muon from W decay. If the axes of all four jets in the event are known, then in general the signal muon has the largest transverse momentum with respect to any of these jet axes.

5 Global variables useful for background separation.

In stop pair production the two neutralinos and the energetic neutrino from the W boson decay escape detection. The simulation with PYTHIA6 allows us to estimate the missing energy and the missing transverse momenta that are carried away by these particles. We also take into account the non-instrumented region around the beam pipe given by the polar angle intervals $\Theta < 7^\circ$ and $\Theta > 173^\circ$.

The distributions of the total missing $E_{miss-tot}$ energy for stop production and top production are presented in **a)** and **b)** plots of Fig.17, respectively. In stop pair production, see plot **a)**, the $E_{miss-tot}$ spectrum starts at 200 GeV. In top pair production (plot **b)**), where two neutralinos are not present, the missing energy $E_{miss-tot}$ is much smaller, going from ≈ 10 GeV to ≈ 260 GeV.

Figure 18 shows the distributions of the total visible energy in the event, $E_{vis-tot}$, in stop production (plot **a)**) and in top production (plot **b)**). The large missing energy in stop production (Fig.17) is related to the low visible energy (Fig.18), while in top

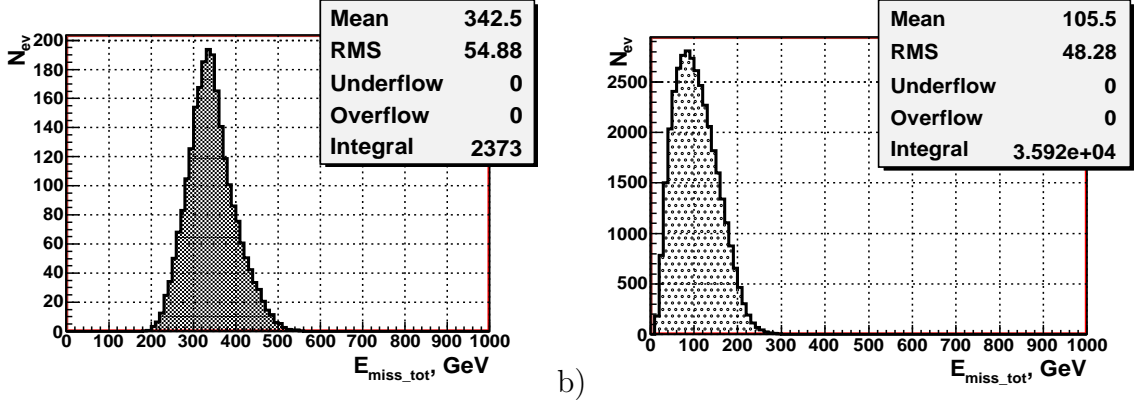


Figure 17: Missing energy $E_{miss-tot}$ distribution. a) stop pair production; b) top pair production.

production the low missing energy correlates with the large visible energy. A cut on the total visible energy of approximately $E_{vis-tot} < 220$ GeV² would eliminate almost completely the top background, while leaving the most part of the signal events.

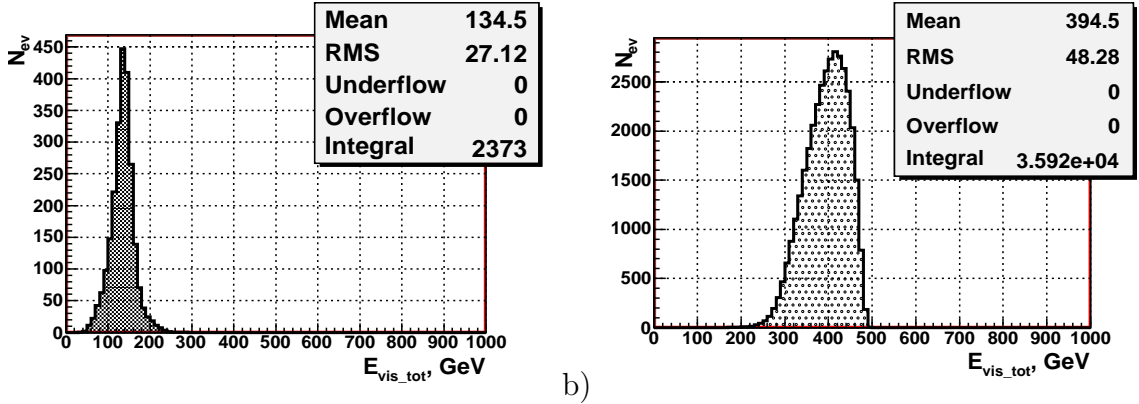


Figure 18: Total visible energy $E_{vis-tot}$ distribution. a) stop pair production; b) top pair production.

Another useful observable is the scalar sum of the moduli of the transverse momenta in an event $PT_{scalsum} = \sum_{i=1}^{N^{part}} |PT_i|$, where the sum goes over all (N^{part}) detectable particles in the event. Figure 19 shows the distributions of the scalar sum of the transverse momenta for the stop production (plot a)) and for top production (plot b)). It is seen that the restriction $PT_{scalsum} \leq 150$ GeV would lead to a good separation of the stop signal events from the top background.

Let us consider also the invariant mass of the system that contains all observable objects in the final state. This invariant mass is the modulus of the vectorial sum of the 4-momenta P_{jet}^n ³ of all ($N^{jet} = 4, n = 1, 2, 3, 4$) jets³ in an event plus the 4-momentum of the signal muon P_μ ,

²That is equivalent to setting a lower limit for the missing energy.

³ The 4-momentum $P^n = (P_0^n, \mathbf{P}^n)$, of the n-th jet includes its energy $P_0^n = E^n$ and the components of the 3-dimensional momentum $\mathbf{P}^n = (P_x^n, P_y^n, P_z^n)$.

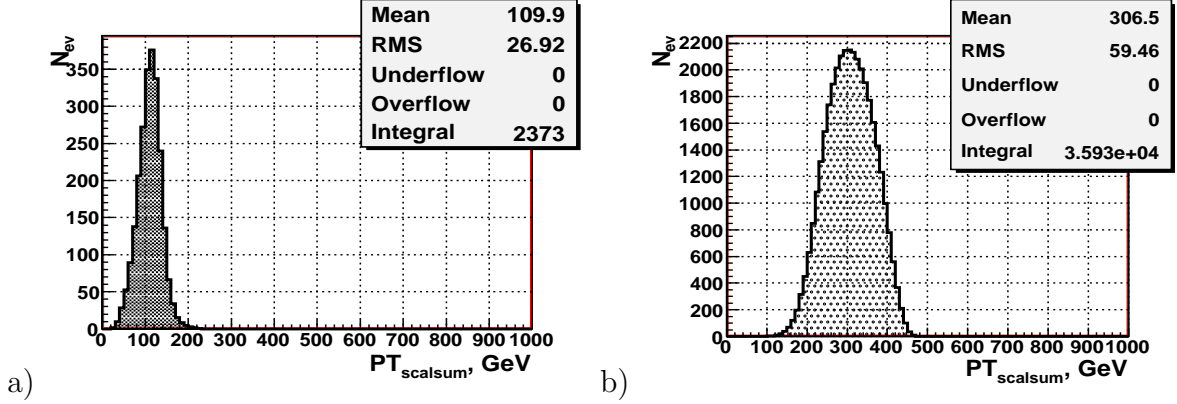


Figure 19: $PT_{scalsum}$ - distribution. a) stop pair production; b) top pair production.

$$M_{inv}(Alljets, \mu) = \sqrt{(\sum_{n=1}^{N^{jet}} P_{jet}^n + P_{\mu})^2}. \quad (11)$$

The distribution of this invariant mass is shown in Fig.20. Plot a) shows the results for stop pair production while plot b) is for top pair production. As seen from these plots, the cut $M_{inv}(Alljets, \mu) \leq 200$ GeV will give a good separation of signal stop and top background events.

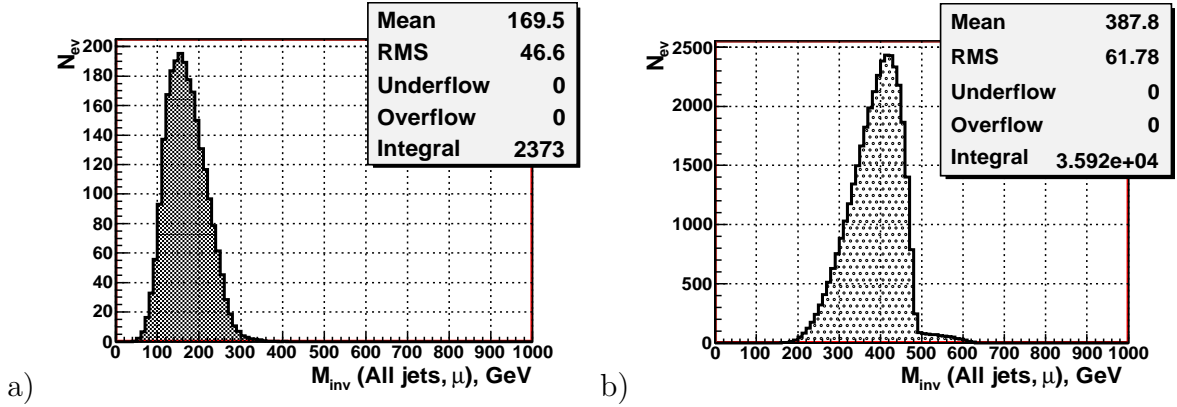


Figure 20: Distribution of number of events, N_{event} ($L_{int} = 1000 fb^{-1}$), versus the reconstructed invariant mass of all jets and signal muon $M_{inv}(Alljets, \mu)$. a) stop pair production; b) top pair production.

6 Global jet variables and cuts.

An even more efficient separation of the signal and the background can be obtained by using the invariant mass of all jets $M_{inv}(Alljets)$ which is the modulus of the vectorial sum of the 4-momenta of all N^{jet} jets in an event

$$M_{inv}(Alljets) = \sqrt{(\sum_{n=1}^{N^{jet}} P_{jet}^n)^2}. \quad (12)$$

The distribution of this invariant mass is shown in Fig.21. Plot **a)** presents the result for stop pair production while plot **b)** that for top pair production. It is seen that the application of the cut $M_{inv}(Alljets) \leq 160$ GeV leads to practically a complete separation of signal stop and top background events.

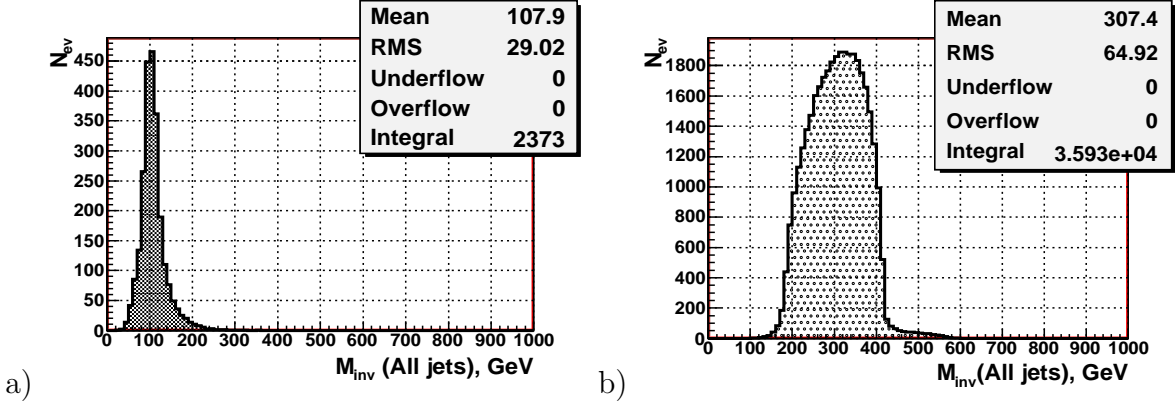


Figure 21: *Distribution of number of events, N_{ev} ($L_{int} = 1000fb^{-1}$), versus the reconstructed invariant mass of all jets $M_{inv}(Alljets)$. **a)** stop pair production; **b)** top pair production.*

Another variable that can also be used for the separation of the signal and the background is the "missing" mass $M_{missing}$ (we use $\sqrt{s} = 500$ GeV)

$$M_{missing} = \sqrt{(\sqrt{s} - (\sum_{n=1}^{N_{jet}} E_{jet}^n + E_{\mu}))^2 - (\sum_{n=1}^{N_{jet}} \mathbf{P}_{jet}^n + \mathbf{P}_{\mu})^2} \quad (13)$$

This variable takes into account the contribution of those particles that cannot be registered in the detector (neutrinos and neutralinos). The distributions of this invariant "missing" mass are given in Fig.22. Plot **a)** shows the results for stop pair production while plot **b)** is for top pair production. As can be seen from these plots, the cut $M_{missing} \geq 250$ GeV also allows us to get rid of most of the top background contribution.

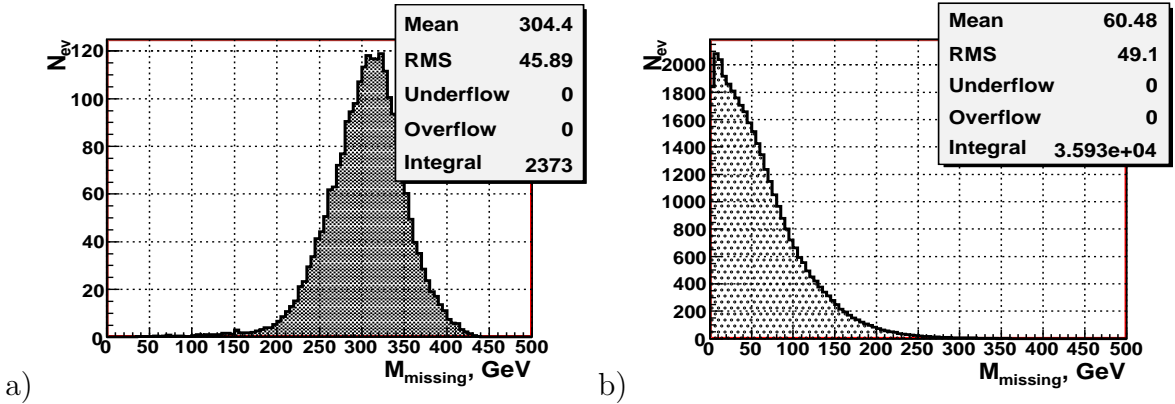


Figure 22: *Distribution of number of events, N_{ev} ($L_{int} = 1000fb^{-1}$), versus the missing mass variable. **a)** stop pair production; **b)** top pair production.*

6.1 Cuts and signal-to-background ratio.

To diminish the influence of jet energy redistribution effect, discussed in subsections 3.2 and 3.3, we shall use the cuts considered above for $M_{missing}$ and $M_{inv}(Alljets)$. These variables, by definition, include the total 4-momentum of all jets, defined as the vectorial sum of the 4-momenta of all jets. Therefore they do not suffer from energy redistribution between jets. Consequently, we use the following three cuts to separate the signal and background events:

- there must be at least two b -jets in an event:

$$N_{b-jets} \geq 2; \quad (14)$$

- the invariant missing mass must be larger than 250 GeV:

$$M_{missing} \geq 250 \text{ GeV}; \quad (15)$$

- the invariant mass of all jets must be smaller than 160 GeV:

$$M_{inv}(Alljets) \leq 160 \text{ GeV}. \quad (16)$$

These three cuts reduce the number of top background events from $\approx 3.5 * 10^4$ to ≈ 12 and the number of stop signal events from 2373 to 1806. So, the cuts improve the signal-to-background ratio from $S/B = 0.066$ to $S/B \approx 143$ losing about 23.8% of the signal stop events. The efficiency values for the cuts (14)–(16) are calculated for $\sqrt{s} = 500$ GeV. We define them as the summary efficiencies. It means that if ε_1 is the efficiency of the first cut (14), ε_{12} is the efficiency of applying the first cut (14) and then second cut (15). Analogously, ε_{123} is the efficiency of the successive application of the cuts (14), (15) and (16). The following results are obtained:

$$\begin{aligned} \text{For SIGNAL STOP events:} \quad & \varepsilon_1 = 0.84; \quad \varepsilon_{12} = 0.78; \quad \varepsilon_{123} = 0.76; \\ \text{For BACKGROUND TOP events:} \quad & \varepsilon_1 = 0.94; \quad \varepsilon_{12} = 0.001; \quad \varepsilon_{123} = 3.3 \cdot 10^{-4}. \end{aligned}$$

6.2 Signal and background cross sections.

We give the cross sections and the numbers of events for stop pair production and top pair production for five energies \sqrt{s} in Table 1 without cuts and Table 2 with cuts. To calculate the rates of stop production at different energies we take the value of the integrated luminosity $L_{int} = 1000 \text{ fb}^{-1}$ for all energies.

It is seen that the cuts (14)–(16) lead to a strong suppression (more than 3 orders of magnitude) of the background top contribution and a moderate loss of signal stop events produced in the energy range $400 \leq \sqrt{s} \leq 800$ GeV.

For the stop mass chosen, the largest number of signal events is expected at $\sqrt{s} = 500$ GeV. Let us note that, according to [21], a 50% efficiency of the separation of b -jets and 80% of the corresponding purity can be expected. It means that in reality to get 1806 signal stop events, reconstructed with an account of b -tagging, we will need about

2.5 times higher statistics than that provided by the integrated luminosity 1000 fb^{-1} at $\sqrt{s} = 500 \text{ GeV}$.

It is worth noting that, as seen from Table 2, even with the use of the fixed parameters of the cuts (14)–(16) the number of signal stop events that can pass these cuts grows rapidly with the energy in the region $400 \leq \sqrt{s} \leq 500 \text{ GeV}$ where mass measurements will be done in the first phase. These measurements may allow to enlarge the sample of collected signal events and to perform a precise measurement of the stop mass. The region $500 \leq \sqrt{s} \leq 800 \text{ GeV}$, which will be available in the second phase of ILC operation, allows to gain a much higher stop statistics, as seen in Table 2. A complete analysis based on adjusting the parameters of the selection cuts (15)–(16) for each of the above energies intervals will be presented in forthcoming papers.

Table 1: The cross sections and the number of events for stop and top pair production before cuts. $L_{int} = 1000 \text{ fb}^{-1}$ is assumed for each energy

$2E_b = \sqrt{s} \text{ [GeV]}$	$\sigma_{stop}^{e^+e^-} \text{ [fb]}$	N_{stop}^{events}	$\sigma_{top}^{e^+e^-} \text{ [fb]}$	N_{top}^{events}	S/B
350	0.23	233	13.76	13750	0.0169
400	1.34	1347	38.79	38740	0.0347
500	2.37	2378	35.94	35950	0.0661
800	1.89	1809	17.36	17359	0.1042
1000	1.42	1265	11.66	11656	0.1085

Table 2: The same as in Table 1 but after applying cuts (14)–(16).

$2E_b = \sqrt{s} \text{ [GeV]}$	$\sigma_{stop}^{e^+e^-} \text{ [fb]}$	N_{stop}^{events}	$\sigma_{top}^{e^+e^-} \text{ [fb]}$	N_{top}^{events}	S/B
350	0.0089	8	0	0	
400	0.52	521	$2.32 * 10^{-4}$	0.2	2605
500	1.80	1806	$2.26 * 10^{-2}$	12.6	143
800	0.99	995	$1.08 * 10^{-2}$	10	99
1000	0.41	410	$6.26 * 10^{-3}$	6	69

7 Determination of scalar top quark mass.

Another variable of interest is the invariant mass $M_{inv}(b - jet, JETS_W)$:⁴

$$M_{inv}(b - jet, JETS_W) \equiv \sqrt{(P_{b-jet} + P_{JETS_W})^2}, \quad (17)$$

which is constructed as the modulus of the vectorial sum of the 4-momentum P_{b-jet} of the b -jet, plus the total 4-momentum of $JETS_W$ system, i.e., non- b -jets stemming from the W decay ($P_{JETS_W} = P_{jet1_W} + P_{jet2_W}$, as there are only two jets allowed to be produced in W decay). More precisely, if the signal event contains a μ^- as the signal muon (see Fig.1), we have to take the b -jet (\bar{b} -jet in the case of μ^+ as the signal muon). This is

⁴ We follow here the notations of subsections 3.2 and 3.3

only possible if one can discriminate between the b - and \bar{b} -jets experimentally. Methods of experimental determination of the charge of the b -jet (\bar{b} -jet) were developed in [21]. In the present paper we do not use any b -tagging procedure. The PYTHIA information about quark flavor is taken for choosing the b - and \bar{b} -jets.

The distributions of the invariant mass of the " b -jet+ $JETS_W$ " system is shown in Fig.23. Their analogs $M_{inv}(b, 2 \text{ quarks}_W)$, obtained at quark level, are presented in Fig.24. Plots **a**) of these two Figures show the results for stop pair production while plots **b**) are for top pair production. These distributions are obtained without any cuts.

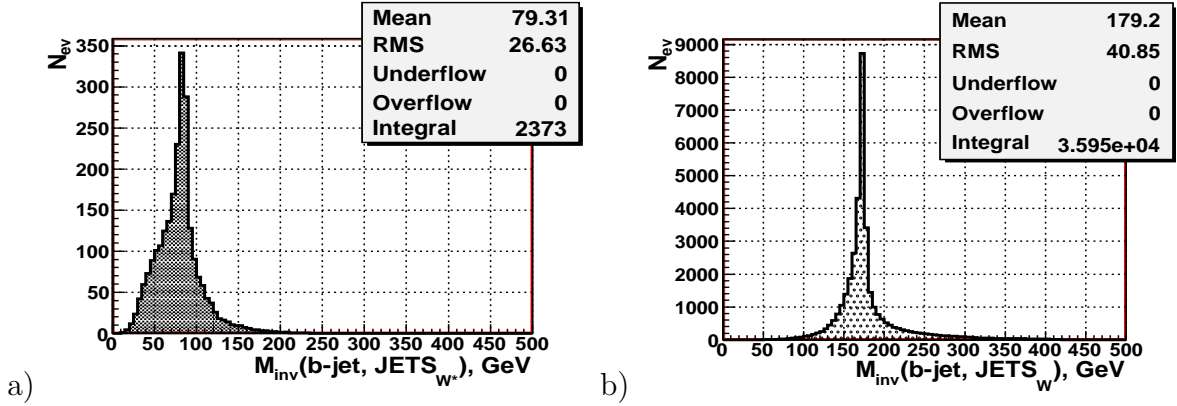


Figure 23: The spectra of the invariant masses $M_{inv}(b - jet, JETS_W)$ before the cuts (14) - (16). **a**) stop pair production; **b**) top pair production.

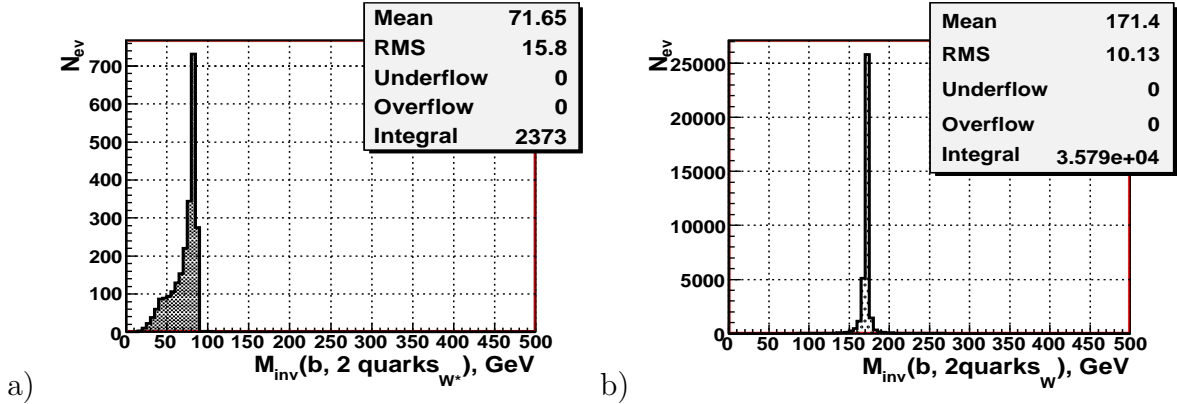


Figure 24: The spectra of the invariant masses $M_{inv}(b, 2 \text{ quarks}_W)$ before the cuts (14) - (16). **a**) stop pair production; **b**) top pair production.

In the top case the invariant mass $M_{inv}(b, 2 \text{ quarks}_W)$ of the system composed of a b -quark and two quarks from W decay should reproduce the mass of their parent top quark (see Fig.1). The distributions of events $dN^{event}/dM_{inv}/5 \text{ GeV}$ expected in each bin of 5 GeV versus the invariant mass $M_{inv}(b, 2 \text{ quarks}_W)$ of the parent three quarks as well as the invariant mass of jets produced by these quarks, i.e. $M_{inv}(b - jet, JETS_W)$, are shown for jet and quark levels in plots **b**) of Fig.23 and 24, respectively, for an integrated luminosity of 1000 fb^{-1} . These distributions have an important common feature. Namely, they show that the peak positions at quark level and at jet level, practically coincide

to a good accuracy with each other as well as with the input value of the top quark mass $M_{top} = 170.9(\pm 1.8)$ GeV. It is also seen from plot **b)** of Fig.23 that the quark hadronization into jets leads to a broadening of very small tails which are seen in the invariant mass distribution at quark level (plot **b)** of Fig.24). The right tail, which appeared at jet level (see plot **b)**) of Fig.23 is a bit lower than the left tail and is longer than the left one. One may say that the peak shape at jet level still looks more or less symmetric. The main message from these plots is that the appearance of tails due to quark fragmentation into jets does not change the position of the distribution peak, which allows us to reconstruct the input top mass both at quark and jet levels.

An analogous stability of the peak position at the jet and quark levels for the stop case can be seen in the plots **a)** of Figs.23 and 24. Note that, according to the stop decay chain (2), the right edge of the peak of the invariant mass distribution of the "b + 2quarks_W" system (see plot **a)** of Fig.24) corresponds to the mass difference $M_{\tilde{t}_1} - M_{\tilde{\chi}_1^0}$.

Now let us recall that according to subsection 6.1 the application of the cuts (14)–(16) leaves only 12 background top events and saves about 76% of signal stop events. It means that the picture shown in plot **b)** of Fig.23 would change drastically and resemble a random distribution of the twelve top events in a rather wide interval⁵. In the case of stop pair production the distributions of the invariant mass of the "b + 2quarks_W" at quark level and of the system "b-jet+JETS_W" at jet level system are shown in Fig.25 taking only those stop events that have passed the cuts (14)–(16).

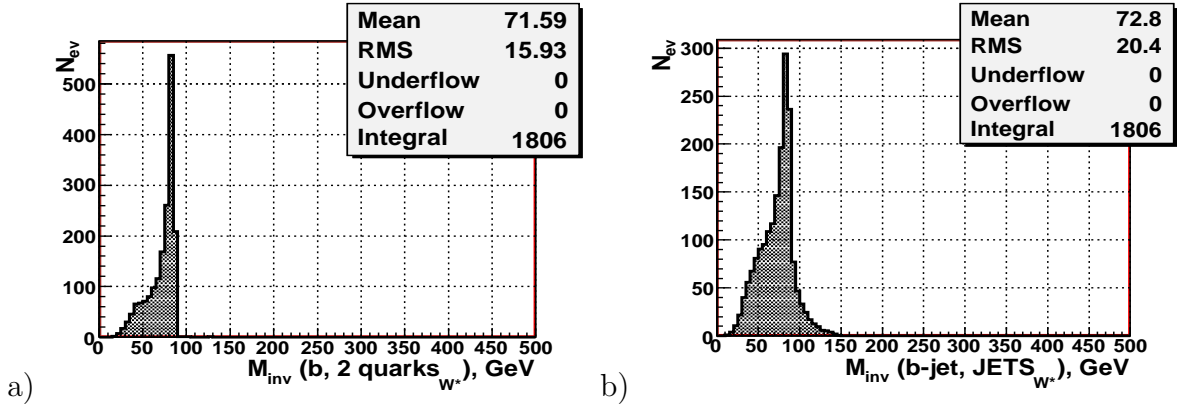


Figure 25: The spectra of the stop signal events ($L_{int} = 1000 fb^{-1}$) after the cuts (14) - (16), versus the invariant mass $M_{inv}(b\text{-jet}, JETS_{W^*})$. **a)** at quark level, **b)** at jet level.

It is seen that the peak position of the stop distribution at jet level $M_{inv}(b\text{-jet}, JETS_{W^*})$, obtained after application of the cuts (14)–(16) (plot **b)** of Fig.25), coincides with the peak position at quark level (plot **a)** of Fig.25) as well as with the peak positions in plots **a)** of Figs.23 and 24 obtained without any cuts. Let us note that the observed stability of the peak position in both plots of Fig.25 is due to the rather moderate loss of the number of events in the peak region (they change from ≈ 550 to ≈ 290) while passing from quark level to jet level. The interval 150–350 GeV in the plot **b)** of Fig.25 can be used to calculate the width between the grid dots in this plot. It is found to be about 7.4 GeV. This number allows to estimate the position of the right edge of the peak

⁵ for more details see Section 8

of $M_{inv}(b\text{-jet}, JETS_{W^*})$ distribution, which seems to be shifted to the left side from 100 GeV point by the distance which is a bit less than two dot intervals, i.e., by a bit less than 14.8 GeV. Thus, we can estimate that the right edge of the $M_{inv}(b\text{-jet}, JETS_{W^*})$ distribution peak lies a bit higher than 85.2 GeV.

Some remarks about the tails in the stop distributions are in order now. The origin of the right and left tails of the distribution shown in the plot **a)** of Fig.25 can be clarified by the results of the stop mass reconstruction by calculating its invariant mass at quark level $M_{inv}(b, 2 \text{ quarks}_{W^*}, \tilde{\chi}_1^0)$ as the modulus of the sum of the 4-momenta of all three quarks and the neutralino (see Fig.1) in stop decay. These results are given in plot **a)** of Fig.26 which shows a very precise reconstruction of the input stop mass at quark level withing the 5 GeV width of the bin containing the peak. Comparing plot **a)** of Fig.25 with plot **a)** of Fig.26 one can conclude that at quark level the long left tail as well as the very small right tail in the distribution of $M_{inv}(b, 2 \text{ quarks}_{W^*})$ disappear when neutralino 4-momentum is added to the 4-momentum of the "b + 2quarks_W" system.

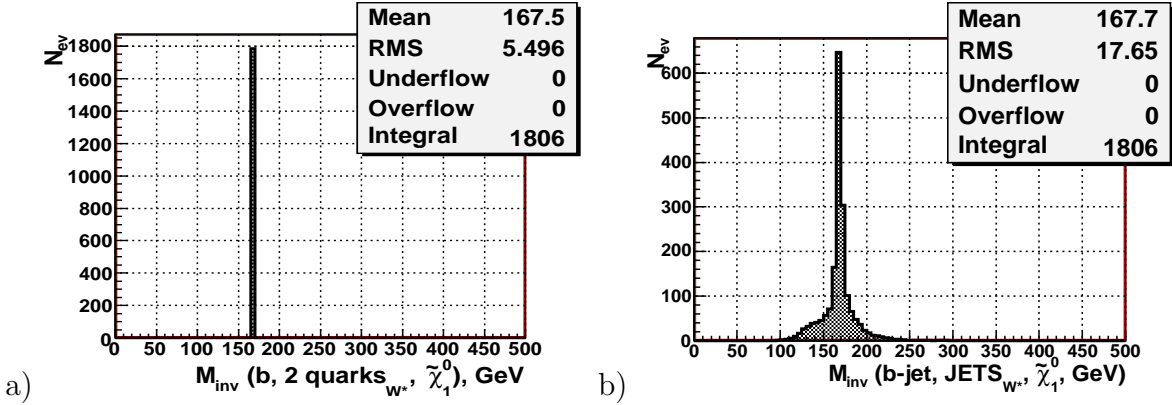


Figure 26: The spectra of the stop signal events after cuts ($L_{int} = 1000 \text{ fb}^{-1}$) versus the invariant mass $M_{inv}(b\text{-jet}, JETS_{W^*}, \tilde{\chi}_1^0)$. **a)** at quark level **b)** at jet level.

The influence of the effect of the hadronization of the b -quarks and of the quarks from W decay into jets is shown in plot **b)** of Fig.26. This plot demonstrates that the hadronization of quarks into jets does not change the position of the stop mass peak, which practically coincides with the input value $M_{\tilde{t}_1} = 167.9$ GeV. It is also seen that the hadronization results in the appearance of more or less symmetrical and rather suppressed short tails around the peak position. The mean value of the distribution in plot **b)** of Fig.26 is also very slightly different from the mean value of the quark level distribution shown in plot **a)** of Fig.26. Both of these mean values are in a good agreement with the input value of the stop mass. It is worth mentioning that the shape of the peak in the stop plot **b)** of Fig.26 looks similar to the shape of the peak in the top plot **b)** of Fig.23 which also demonstrates the stability (compared to the quark level top plot **b)** of Fig.24) of the reconstructed top mass peak position after taking into account the effect of quark fragmentation to hadrons.

It is seen from plot **b)** of Fig.25 that by adding the mass of the neutralino $M_{\tilde{\chi}_1^0} = 80.9$ GeV to the value of the right edge point of the peak $M_{inv}(b\text{-jet}, JETS_{W^*}) \approx 85.2$ GeV one can get the lower limit for the reconstructed stop mass $M_{\tilde{t}_1}^{reco-low} \approx 166.2$ GeV which reproduces well the input value $M_{\tilde{t}_1} = 167.9$ GeV.

The simulation has shown (see plot **b**) of Fig.27) that the 12 background top events, which have passed our cuts (14)-(16), as discussed above, are mostly distributed in the region $30 \leq M_{inv}(b\text{-jet}, JETS_W) \leq 140$ GeV. This region is by more than twenty times wider than the 5 GeV width of the peak interval in the $M_{inv}(b\text{-jet}, JETS_W)$ distribution which is shown in plot **b**) of Fig.25 for the stop and which contains about 290 signal stop events left after the cuts. Therefore, we expect that in future measurements the contribution of these twelve remaining top background events will not influence the position of the peak of the $M_{inv}(b\text{-jet}, JETS_W)$ distribution (shown in plot **b**) of Fig.25) which allows one to reconstruct the input value of the stop mass by adding the mass of the neutralino.

8 Results for top squark mass $M_{\tilde{t}_1} = 200$ GeV.

In this section we want to discuss what will change if the mass of the top squark is different from the one we have chosen. In the present paper we have chosen a rather low scalar top quark mass (one of the lowest stop quark's masses that is allowed for the case of $\tilde{t}_1 \rightarrow b\tilde{\chi}_1^\pm$ decay channel). With increase of the stop mass the cross section for its production is decreasing. So, for example, for the case of $M_{\tilde{t}_1} = 200$ GeV and the integrated luminosity $L_{int} = 1000 fb^{-1}$ the number of events per year at $\sqrt{s} = 500$ GeV is decreasing to 509 (after the cuts (14)-(16)). The mass $M_{\tilde{t}_1} = 200$ GeV is still below the highest allowed stop mass for the $\tilde{t}_1 \rightarrow b\tilde{\chi}_1^\pm$ decay channel (which is about 255 GeV) corresponding to $M_{\chi_1^+} = 159.2$ GeV and $M_{\chi_1^0} = 80.9$ GeV. For stop masses below and above the described region, the stop will decay to other channels which we do not consider in this paper. The distribution of the invariant mass $M_{inv}(b\text{-jet}, JETS_W)$ of the "b-jet+ $JETS_{W^*}$ " system for events which have passed the same cuts (14)-(16) is shown in Fig.27. Plot **a**) is for stop production with $M_{\tilde{t}_1} = 200$ GeV, plot **b**) is for top production. The top background also remains the same as it was given in Table 2 for $\sqrt{s} = 500$ GeV, i.e., about 12 events.

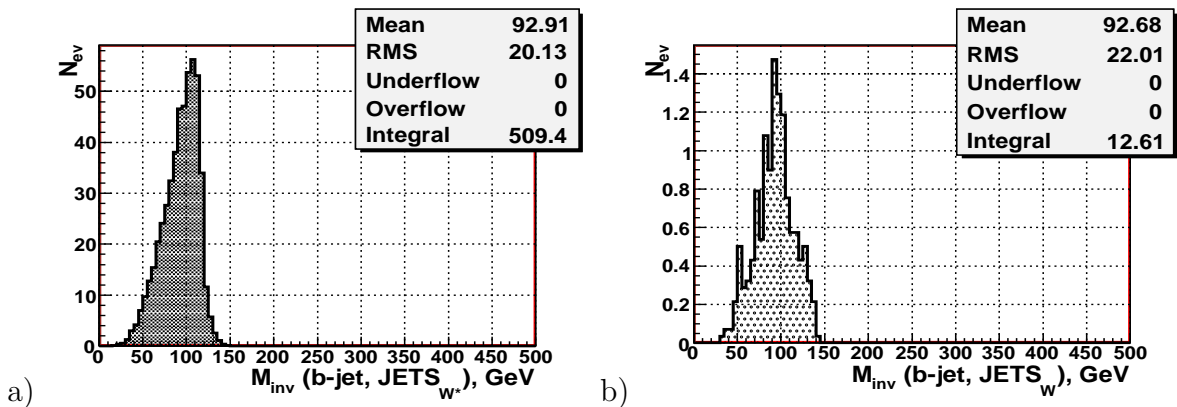


Figure 27: The spectra of the invariant masses $M_{inv}(b_{jet}, JETS_W)$ of the "b-jet+(all-non-b-jets)" system after cuts ($L_{int} = 1000 fb^{-1}$). **a**) stop pair production; **b**) top pair production.

The distribution in plot **a**) has a peak at $M_{inv}(b\text{-jet}, JETS_{W^*}) \approx 110$ GeV. One can also determine the mass of the stop quark following the procedure described in Section 7, but with less accuracy than in the case of the lower stop mass used in previous Sections.

9 Conclusion.

We have studied stop pair production in electron-positron collisions within the framework of the MSSM for the total energies $\sqrt{s} = 350, 400, 500, 800, 1000$ GeV. We assume that the stop quark decays dominantly into a chargino and a b -quark, $\tilde{t}_1 \rightarrow b\tilde{\chi}_1^\pm$, and the chargino decays into a neutralino and a W boson, $\tilde{\chi}_1^\pm \rightarrow \tilde{\chi}_1^0 W^\pm$, where the W boson is virtual. One of the two W's decays hadronically, $W^+ \rightarrow q\bar{q}$, the other one decays leptonically, $W^- \rightarrow \mu^- \nu$.

We have performed a detailed study based on a Monte Carlo simulation with the program PYTHIA6.4 for $E_{e^+e^-}^{tot} = \sqrt{s} = 500$ GeV and an integrated luminosity 1000 fb^{-1} . At this energy we expect the highest number of the signal events for the chosen stop mass $M_{\tilde{t}_1} = 167.9$ GeV. The program CIRCE1 is used to get the spectra of electron (positron) beams taking into account the effects of beamstrahlung. PYTHIA6.4 is used to simulate stop pair production and decay as well as top pair production being the main background.

Three cuts (14)-(16) have been proposed to separate signal stop events and top background events. For $\sqrt{s} = 500$ GeV and the luminosity 1000 fb^{-1} they give 1806 signal stop events with 12 background top events. This is different from the more complicated situation in stop pair production at LHC (see, for instance, [20]).

We have shown that the determination of the right edge of the peak position of the invariant mass $M_{inv}(b\text{-jet}, JETS_{W^*})$ distribution of the "b-jet+(all-non-b-jets)" system allows us to measure the mass of the stop quark with a good accuracy based on the statistics corresponding to an integrated luminosity of 1000 fb^{-1} . For this the mass of χ_1^0 has to be known.

As seen from the Table 2 the measurements at other energies in the regions $400 \leq \sqrt{s} \leq 500$ GeV and $500 \leq \sqrt{s} \leq 800$ GeV may allow to enlarge substantially the number of selected signal stop events and to perform a precise measurement of the mass of the scalar top quark.

In the last Section we discussed the difference in the main invariant distribution for a $M_{\tilde{t}_1} = 200$ GeV.

In conclusion we can say that the e^+e^- channel together with the $\gamma\gamma$ channel considered in our previous Note [6] is well suited for the study of stop pair production at ILC.

10 Acknowledgements.

This work is supported by the JINR-BMBF project and by the "Fonds zur Förderung der wissenschaftlichen Forschung" (FWF) of Austria, project No.P18959-N16. The authors acknowledge support from EU under the MRTN-CT-2006-035505 and MRTN-CT-2004-503369 network programmes. A.B. was supported by the Spanish grants SAB 2006-0072, FPA 2005-01269 and FPA 2005-25348-E of the Ministerio de Educacion y Ciencia.

References

- [1] Y.Gol'fand and E.Likhtman, JETP Lett. 13(1971) 323;

- D.Volkov and V.Akulov, Phys.Lett. B46(1973) 109;
 J.Wess and B.Zumino, Nucl.Phys. B70(1974) 39.
- [2] J.Ellis and S.Rudaz, Phys.Lett. B128(1983) 248.
- [3] G.Altarelli and R.Rückl, Phys.Lett. B144(1984) 126;
 S.Dawson, E.Eichten and C.Quigg, Phys.Rev. D31(1985) 1581;
 K.Hikasa and M.Kobayashi, Phys.Rev. D36(1987) 742;
 M.Drees and K.Hikasa, Phys.Lett. B252(1990) 127;
 J.Ellis, G.L.Fogli and E.Lisi, Nucl.Phys. B393(1993) 3.
- [4] ILC Reference Design Report, v.1 "Executive Summary",
 Editors: J.Brau, Y.Okada, N.Walker, 2007;
<http://www.linearcollider.org/cms/?pid=1000025>.
- [5] ILC Reference Design Report, v.2 "Physics at the ILC",
 Editors: A.Djouadi, J.Lykken, K.Mönig, Y.Okada, M.Oreglia, S.Yamashita, 2007;
<http://www.linearcollider.org/cms/?pid=1000025>.
- [6] A.Bartl, K.Mönig, W.Majerotto, A.Skachkova, N.Skachkov,
 "Pair Production of Scalar Top Quarks in Polarized Photon-Photon Collisions at ILC", ILC-NOTE-2007-036, arXiv:0804.1700[hep-ph].
- [7] A.Bartl, H.Eberl, S.Kraml, W.Majerotto and W.Porod, Eur.Phys.J.C2(2000)6;
 hep-ph/0002115.
- [8] A.Bartl, K.Moenig, W.Majerotto, A.Skachkova, N.Skachkov,
 "Stop pair production in polarized photon-photon collisions",
 Proc. of the Intern. Conf. on Linear Colliders (LCWS 2004), vol.II, p.919, April
 19-23, 2004, Le Carre des Sciences, Paris, France.
- [9] A.Finch, H.Nowak and A.Sopczak, hep-ph/0211140.
- [10] M.Carena et.al, Phys.Rev. D72:115008, 2005; hep-ph/0508152.
- [11] A. Sopczak et.al, hep-ph/0605225.
- [12] T. Sjöstrand, S. Mrenna and P.Skands JHEP 0605:026, 2006; hep-ph/0603175v2
- [13] T. Ohl, "κ_lρκ_η Version 1.0: Beam Spectra for Simulating Linear Collider Physics",
 hep-ph/9607454.
- [14] J.F.Gunion, H.E.Haber, Nucl.Phys. B272(1986)1; B278(1986)449; Erratum
 B402(1993)567.
- [15] E. Brubaker et al. "Combination of CDF and D0 results on the mass of the
 top quark"; By Tevatron Electroweak Working Group, Fermilab-TM-2380-E, 19
 Mar2007; arXiv:hep-ex/0703034.
- [16] S.Catani, Yu.L. Dokshitzer, M.Olson, G.Turnock and B.Webber, Phys.Lett. B269
 (1991) 432.

- [17] JADE Collab., W.Bartel et al. *Z.Phys. C*33 (1986) 23; S.Bethke, Habilitation thesis, LBL, 50-208, 1987.
- [18] G.Klamke and K.Moenig, *Eur.Phys.J.C*42(2005)261, DESY-05-049, Mar 2005, hep-ph/0503191.
- [19] R.Hawkings, "Vertex detector and flavour tagging studies for TESLA linear collider", LC-PHSM-2000-021, 2000
- [20] U.Dydak, "Search for the stop quark with CMS at the LHC"; CMS TN/96-022, CERN, 1996;
U.Dydak, H.Rohringer and J.Tuominiemi, "Study of the channel gluino \rightarrow stop + top", CMS TN/96-103, CERN, 1996.
- [21] C.J.S.Damerell, D.J.Jackson, eConf960625 (1996) DET078;
R.Hawkings, LC-PHSM-2000-021;
S.M.Xella Hansen, D.J.Jackson, R.Hawkings, C.J.S.Damerell, LC-PHSM-2001-024;
S.M.Xella Hansen, M.Wing, D.J.Jackson, N. De Groot, C.J.S.Damerell, LC-PHSM-2003-061;
S.M.Xella Hansen et al. [Linear Collider Flavour Identification Collaboration], *Nucl.Instrum.Meth.A*501,106(2003); S.Hillert, C.J.S.Damerell, eConf0508141 (2005) ALCPG 1403.
- [22] G.Moortgat-Pick et.al., "The role of polarized positrons and electrons in revealing fundamental interactions at the Linear Collider", *Phys.Rept.*460 (2008) 131; hep-ph/0507011.
- [23] D. Schulte, "Study of electromagnetic and hadronic background in the interaction region of the TESLA Collider, Ph.D. Thesis, Univ. Hamburg, 1997, DESY-TESLA-97-08;
K.Yokoya and P.Chen, KEK Preprint 91-2, April 1991;
http://www-sldnt.slac.stanford.edu/nlc/programs/guinea_pig/gp_index.html.